JOURNAL OF GUIDANCE, CONTROL, AND DYNAMICS
Vol. 32, No. 6, November–December 2009

Minimum-Time Path Planning for Unmanned Aerial Vehicles in Steady Uniform Winds

Laszlo Techy* and Craig A. Woolsey†
Virginia Polytechnic Institute and State University, Blacksburg, Virginia 24061

DOI: 10.2514/1.44580

This paper is concerned with time-optimal path planning for a constant-speed unmanned aerial vehicle flying at constant altitude in steady uniform winds. The unmanned aerial vehicle is modeled as a particle moving at a constant air-relative speed and with symmetric bounds on turn rate. It is known from the necessary conditions for optimality that extremal paths comprise only straight segments and maximum-rate turns. An essential observation is that maximum-rate turns correspond to trochoidal path segments, as observed from an Earth-fixed inertial frame. The path-planning problem therefore reduces to identifying the switching points at which straight and trochoidal path segments join to form a feasible path and choosing the true minimum-time solution from the resulting set of candidate extremals. The paper's primary contribution is a simple analytical solution for a subset of candidate extremal paths: those for which an initial maximum-rate turn is followed by a straight segment and then a second maximum-rate turn in the same direction as the first. The solution is easy to compute and is suitable for real-time implementation onboard an unmanned aerial vehicle with limited computational power. The remaining candidate extremal paths may be found using a simple numerical root-finding routine. The paper also shows that, for some candidate extremal paths, no corresponding Dubins path exists in the (moving) air-relative frame.

Nomenclature

$\mathcal{F}_A$	=	air-relative frame
$\mathcal{F}_I$	=	inertial reference frame
$\mathcal{F}_T$	=	trochoidal frame
$\mathcal{H}$	=	Hamiltonian
$t_{2\pi}$	=	time required for one full turn at maximum turn rate
V_a	=	airspeed of the unmanned aerial vehicle
V_w	=	wind speed
λ	=	adjoint variables
χ	=	course angle
ψ	=	heading angle
ψ_w	=	direction of ambient air's motion
ω	=	turn rate

I. Introduction

THIS paper describes a framework for minimum-time path planning in the horizontal plane. We consider a kinematic model for an unmanned air vehicle (UAV) flying at constant altitude and constant air-relative speed in a steady uniform flowfield. In this setting, we seek the feasible path that brings the UAV from a given initial point and heading to a given final point and heading in the least amount of time. Neglecting the effect of wind, this problem is equivalent to finding the minimum arc-length path of bounded curvature connecting two points in the plane with prescribed initial and final slopes. The problem was formulated and studied by Dubins, who showed, using geometrical considerations, that a minimum-length path contains only maximum-curvature circular arcs and straight segments and, moreover, that it contains three such segments at most [1]. The problem has been reformulated and solved using optimal control theory and Pontryagin's minimum principle in [2]; additional necessary conditions for optimality were provided in [3].

More recently, the preceding methods have been adopted for time-optimal path planning for UAVs traveling in steady uniform winds [4,5]. In these papers, minimum-time trajectories are designed in the air-relative frame $\mathcal{F}_A$, an inertial frame that moves in the direction of the ambient wind with the same speed. The desired final point in inertial space corresponds to a point in $\mathcal{F}_A$, a virtual target, that moves with the same speed as the wind and in the opposite direction. The challenge is to find the point along the virtual target's path at which a Dubins path intercepts the target. The algorithm iteratively solves the Dubins problem in $\mathcal{F}_A$ until the interception error converges to zero.

Alternatively, one may exploit the geometry of the candidate extremal paths and obtain analytical solutions. The key observation is that a UAV flying in a constant ambient wind with a constant maximum turn rate generates a trochoidal path [6] for which analytical expressions exist. Because extremal trajectories may only contain straight paths and trochoidal segments, one may seek the solution in terms of switching points for which a concatenation of such segments yields a feasible path [7]. Independently of this research, the importance of trochoidal trajectories for minimum-time path planning was recognized in [8]; however, only numerical solutions are presented there.

In this paper, we provide a detailed description of the minimum-time path-planning problem in the plane using trochoidal paths and straight segments. In Sec. II, we set up the problem and introduce the trochoidal frame in which the x axis is aligned with the direction of the ambient air's motion. The trochoidal coordinates expressed in this frame are an essential part of the development. In Sec. III, the general character of extremal paths is discussed. We summarize previous results on minimum-time path planning using Pontryagin's minimum principle and provide an additional necessary condition for optimality. Generalizing Dubins's results, we consider only three-segment extremals, which can be grouped into two major categories, as shown in Fig. 1. Borrowing terminology from [9], the bang–singular–bang (or BSB) extremals are those candidate time-optimal paths for which an initial turn is followed by a straight segment followed by a second turn. The solutions for these paths are presented in Sec. IV. When the initial and final turns have the same sense, these paths can be solved for analytically. The results shed light on the character of the BSB paths in general and suggest an efficient numerical root-finding routine to obtain the remaining candidate BSB trajectories. The bang–bang–bang (or BBB) extremals comprise a turn followed by a second turn in the opposite sense, which is followed by a third turn in the same direction as the first. The solution

Received 25 March 2009; revision received 8 July 2009; accepted for publication 11 July 2009.

*Graduate Student, Department of Aerospace and Ocean Engineering; techy@vt.edu. Student Member AIAA.

†Associate Professor, Department of Aerospace and Ocean Engineering; cwoolsey@vt.edu. Associate Fellow AIAA.

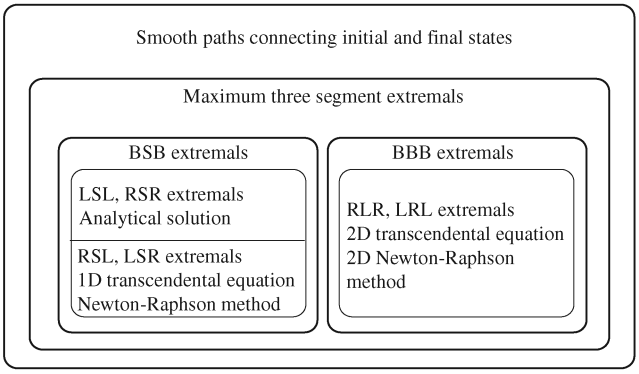

Fig. 1 Venn diagram showing the types of extremals considered in this paper. As in [9], B stands for bang or maximum-rate turn, S stands for straight (also stands for singular), L stands for left, and R stands for right. For example, LSL is an initial left turn, followed by a straight path, then followed by a second left turn.

for these extremals is briefly summarized in Sec. V and is described in more detail in the Appendix. The path-planning algorithm is demonstrated in Sec. VI, in which results are presented for Monte Carlo simulations over a range of randomly selected parameters. Section VII provides conclusions.

II. Problem Formulation

Consider the dynamic system described by the equations

$$\dot{x}_N(t) = V_a \cos\psi(t) + V_x, \qquad \dot{y}_E(t) = V_a \sin\psi(t) + V_y$$
$$\dot{\psi}(t) = u(t) \tag{1}$$

where the components V_x and V_y of the ambient wind are assumed to be constant. The coordinates $x_N(t)$ and $y_E(t)$ describe the vehicle's position in an inertial frame, and $\psi(t)$ describes its heading, measured clockwise from the x_N axis. V_a is the airspeed and $u(t)$ is the turn rate, which we take as a control input.

Suppose the initial and desired terminal conditions are

$$x_N(0) = x_{N_0}, \qquad y_E(0) = y_{E_0}, \qquad \psi(0) = \psi_0 \tag{2}$$

$$x_N(T) = x_{N_f}, \qquad y_E(T) = y_{E_f}, \qquad \psi(T) = \psi_f \tag{3}$$

The objective is to find an extremal control $u^*(t)$ such that the UAV, starting from its initial state, arrives at the desired final state in minimum time. That is, the objective is to find $u^*(t)$ such that the cost function

$$J = \int_0^T \mathrm{d}t = T$$

is minimized subject to the kinematic equations (1) and the symmetric control limits

$$-u_{\max} \le u(t) \le u_{\max}$$

Finding minimum-length paths of bounded curvature was studied by Dubins [1] and was more recently adopted as a means of generating minimum-time paths for constant-speed mobile robots with bounded turn rates, leading to the phrase *Dubins's car* (see [2], for example). One attempt to extend Dubins's results to UAVs in winds is described in [4,5], in which the problem is transformed to a moving reference frame in which the final position becomes a virtual moving target for which the speed is equal and opposite to the wind. Path planning then reduces to a numerical root-finding problem involving iterative solution of the Dubins problem.

This paper presents an alternative approach that uses a simple geometric argument to characterize extremal paths. The result relies on the observation that circular (constant turn rate) UAV paths in the air-relative frame correspond to trochoidal paths in the inertial frame [6]. Following [6], we define a trochoidal frame determined by the wind direction, as shown in Fig. 2.

If χ_w denotes the wind direction (by convention, the direction from which the wind approaches), then $\psi_w = \chi_w \pm \pi$ is the direction of the ambient air's motion. The trochoidal frame $\mathcal{F}_T$ is then defined such that its x axis is oriented downwind, the z axis is into the image, and the y axis completes the right-handed reference frame. Note that the trochoidal frame is fixed relative to the ground, whereas the air-relative frame $\mathcal{F}_A$ is convected downwind. Then the trochoidal coordinates can be found from the inertial coordinates by

$$\begin{pmatrix} x_t(t) \\ y_t(t) \end{pmatrix} = \begin{pmatrix} \cos\psi_w & \sin\psi_w \\ -\sin\psi_w & \cos\psi_w \end{pmatrix} \begin{pmatrix} x_N(t) \\ y_E(t) \end{pmatrix}$$

The kinematic equations expressed in the trochoidal frame are

$$\dot{x}_t(t) = V_a \cos(\psi(t) - \psi_w) + V_w \tag{4}$$

$$\dot{y}_t(t) = V_a \sin(\psi(t) - \psi_w) \tag{5}$$

$$\dot{\psi}(t) = u(t) \tag{6}$$

where $V_w = \sqrt{V_x^2 + V_y^2}$. We assume that $V_w < V_a$, to ensure that feasible solutions exist. In the case of a turn at constant maximum rate $\omega = |\dot{\psi}_{\max}|$, the equations can be rewritten as

$$\dot{x}_t(t) = V_a \cos(\delta\omega t + \phi_t) + V_w \tag{7}$$

$$\dot{y}_t(t) = V_a \sin(\delta\omega t + \phi_t) \tag{8}$$

where $\phi_t = \psi(0) - \psi_w$ and $\delta \in \{-1, 1\}$ describes the direction of the turn. The position of a point on the trochoidal path can then be written as

$$x_t(t) = \frac{V_a}{\delta\omega} \sin(\delta\omega t + \phi_t) + V_w t + x_{t_0} \tag{9}$$

$$y_t(t) = -\frac{V_a}{\delta\omega} \cos(\delta\omega t + \phi_t) + y_{t_0} \tag{10}$$

The trochoidal path defined here is essential in developing the path-planning algorithm described in later sections.

III. Properties of Extremal Paths

In this section, necessary conditions are derived for time optimality. Following [2], we begin with Eqs. (1) and initial

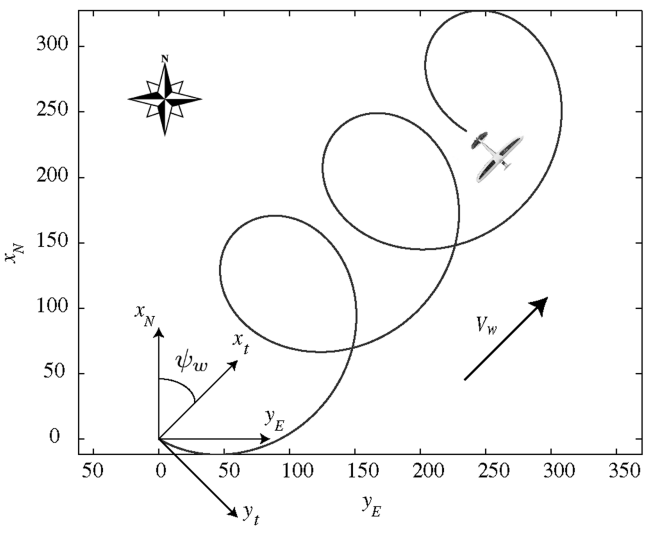

Fig. 2 Trochoidal path and trochoidal frame.

conditions (2). Assume that the coordinates are already expressed in the trochoidal frame such that $V_y = 0$ and $V_x = V_w$. The Hamiltonian for the time-optimal control problem is

$$\mathcal{H} = 1 + \lambda_1(V_a \cos\psi(t) + V_w) + \lambda_2 V_a \sin\psi(t) + \lambda_3 u$$

where $u \in \mathcal{U}$ and $\mathcal{U} = [-u_{\max}, u_{\max}]$ is the set of admissible controls. The costate equations are

$$\dot{\lambda}_1 = 0, \qquad \dot{\lambda}_2 = 0, \qquad \dot{\lambda}_3 = \lambda_1 V_a \sin\psi(t) - \lambda_2 V_a \cos\psi(t)$$

which implies that λ_1 and λ_2 are constant. The minimum principle states that along an extremal trajectory,

$$\mathcal{H}(x^*, u^*, \lambda^*, t) \le \mathcal{H}(x^*, u, \lambda^*, t)$$

for all $u \in \mathcal{U}$ and $0 \le t \le T$. First assume that $\lambda_3 \neq 0$. To satisfy Pontryagin's minimum principle, one needs $u = -\text{sign}(\lambda_3)u_{\max}$ (which is a maximum-rate turn to the left or right) a maximum effort, or bang–bang control. Next, consider the case in which $\lambda_3 \equiv 0$. Because λ_1 and λ_2 are constant, the vector λ is a constant vector. Moreover, because by Pontryagin's minimum principle λ must be nonzero (see also [2]), the third adjoint equation implies that

$$\lambda \| \begin{pmatrix} \cos\psi(t) \\ \sin\psi(t) \\ 0 \end{pmatrix}$$

It follows that $\psi(t)$ must be constant, which corresponds to a straight path. Thus, the time-optimal path consists of turns at maximum rate and straight segments. Extremal trajectories (or extremals) therefore comprise trochoidal and straight segments. In the absence of winds ($V_w = 0$), these trajectories simplify to circular segments and straight lines, and they are often referred to as Dubins paths. As proved in [1], in that case there are six possibilities to connect initial and final oriented points with minimum arc-length paths. (For constant-speed motion, minimum time is equivalent to minimum arc length.) Let L denote a segment corresponding to a maximum-rate turn to the left and let R denote a segment corresponding to a maximum-rate turn to the right. Finally, let S denote a straight segment (which is a singular arc of an extremal path). Generically, the six possible extremal paths are LSL, RSR, LSR, RSL, RLR, and LRL. Finding these candidate paths is a simple geometric exercise; one only needs to find tangents to oriented circles of minimum turn radius. The LRL and RLR paths only exist if the distance between the initial and final points, d, satisfies $d \le 4R_0$, where R_0 is the maximum-rate turning radius. The paths LSR and RSL fail to exist when $d < 2R_0$. In case of equality, $d = 2R_0$, the intermediate straight segment vanishes [4].

Generalizing Dubins's results to the case in which winds are present, we seek trajectories that can be constructed by joining three segments according to BSB or BBB (where B can be either L or R). In Sec. IV, a method is presented to solve for BSB trajectories. The LSL and RSR trajectories can be found analytically; the LSR and RSL trajectories can be found using a simple root-finding method. In Sec. V, a method to find the BBB trajectories is discussed. The true minimum-time solution is found by comparing the transit times for all candidates. The numerical root-finding algorithm described in this paper differs from earlier numerical methods: the framework presented in this work yields closed-form expressions in the form of one or two transcendental equations that have to be solved for one or two unknown parameters, respectively. The known form of the transcendental equations and the insight gained through the development of the analytical expressions allow one to formulate a numerical analysis problem that can be solved efficiently for these unknown parameters.

The number of possible solutions can be confined to a small finite set by introducing a new necessary condition for optimality. Toward that end we express Eqs. (4–6) using the inertial ground speed and course angle instead of the air-relative speed and heading angle:

$$\dot{x}_N(t) = V_g(\psi)\cos(\chi(\psi)) \tag{11}$$

$$\dot{y}_E(t) = V_g(\psi)\sin(\chi(\psi)) \tag{12}$$

$$\dot{\psi}(t) = u(t) \tag{13}$$

where the ground speed $V_g(\psi)$ and the course angle $\chi(\psi)$ depend on the heading angle ψ as follows:

$$V_g(\psi) = \sqrt{V_a^2 + V_w^2 + 2V_a V_w \cos(\psi)} \tag{14}$$

$$\chi(\psi) = \tan^{-1}\left(\frac{V_a \sin\psi}{V_a \cos\psi + V_w}\right) \tag{15}$$

Here, the 4-quadrant inverse tangent function is used. The relationship between course angle and heading angle is illustrated in Fig. 3.

Lemma 1. Consider the kinematic equations (11–13). The heading angle $\psi(t) \in [0, 2\pi)$ and course angle $\chi(\psi(t)) \in [0, 2\pi)$ are in one-to-one correspondence if and only if $V_a > V_w$.

Proof: If $V_a \le V_w$, then the mapping from $\psi(t) \in [0, 2\pi)$ to $\chi(\psi(t))$ is not one to one. Referring to the left side of Fig. 3, the course angle $\chi(\psi(t))$ will only take values for which the ground-relative velocity vector $V_g(\psi(t))$ has a nonnegative x component. It follows that

$$\chi(\psi(t)) \in \left[-\frac{\pi}{2}, \frac{\pi}{2}\right]$$

for $\psi(t) \in [0, 2\pi)$.

If $V_a > V_w$, then from Eq. (15) we can conclude that the denominator of the argument of the arctan function takes values in $[-V_a + V_w, V_a + V_w]$. The numerator takes values in $[-V_a, V_a]$. Moreover, $\chi(\psi(t))$ takes a unique value in $[0, 2\pi)$ for each $\psi(t) \in [0, 2\pi)$, as can be seen in the right side of Fig. 3. □

Lemma 2. Consider an extremal that contains a trochoidal segment, described by Eqs. (9) and (10). Assume that the trochoidal segment begins at point P_0 at path parameter value t_0 and ends at point P_3 corresponding to path parameter value t_3. A necessary condition for optimality is that $\Delta t = (t_3 - t_0) < 2t_{2\pi}$, where

$$t_{2\pi} = \frac{2\pi}{\omega} = \frac{2\pi}{|\dot{\psi}_{\max}|}$$

is the time required for the air-relative velocity vector to describe a full revolution.

Proof: To prove by contradiction, assume that there exists a solution for which $\Delta t \ge 2t_{2\pi}$, corresponding to an optimal trajectory. In that case, the trochoidal path contains at least two full loops. By Lemma 1, there exists a point P_1 and corresponding path parameter value t_1 ($t_0 \le t_1 \le t_0 + t_{2\pi}$) such that the course angle along the path is aligned with the ambient wind's motion at point P_1. Define point P_2 to correspond to path parameter value t_2, where $t_2 = t_1 + t_{2\pi}$. The inertial velocities at points P_1 and P_2 align with the wind vector and with the line segment connecting the two points by Eqs. (7–10); therefore, the trochoidal segment between points P_1 and P_2 can be replaced by a straight path in the direction of the ambient wind's motion (see Fig. 4). The distance from point P_1 to P_2 along the trochoidal segment is

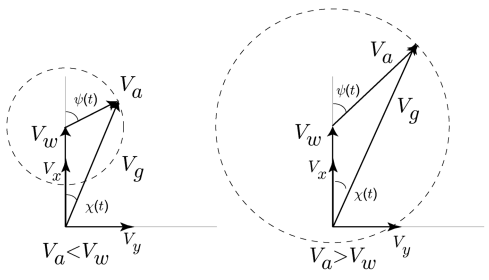

Fig. 3 Relationship between airspeed, wind speed, and ground speed.

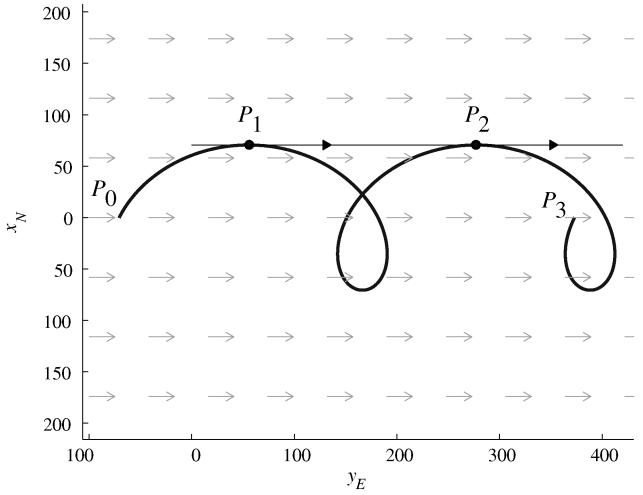

Fig. 4 Time the UAV spends on an extremal trochoidal segment has to be less than $2t_{2\pi}$.

$$D = V_w t_{2\pi} = \frac{V_w}{V_a} 2\pi R_0$$

where $R_0 = V_a/\omega$ is the (constant) minimum turn radius in the air-relative frame. The time it takes to travel on the straight line instead of the trochoid is $t_s = D/(V_w + V_a)$, because the tangent line connecting points P_1 and P_2 has to be aligned with the wind vector. Thus,

$$t_s = \frac{V_w}{V_a + V_w} t_{2\pi} < t_{2\pi}$$

Consequently, the trochoidal segment can be replaced by the shorter straight segment. Because a trajectory can only be optimal if all subtrajectories are optimal as well, it follows that the original trochoidal path cannot be optimal; thus, $\Delta t < 2t_{2\pi}$ is a necessary condition for optimality. □

IV. Solving for BSB Trajectories

Given the initial and final conditions (2) and (3), we define two trochoids $(x_{t_1}(t), y_{t_1}(t))^T$ and $(x_{t_2}(t), y_{t_2}(t))^T$ as in Eqs. (9) and (10), such that the first trochoid satisfies the initial conditions (2) at $t = 0$ and the second trochoid satisfies the final conditions (3) at $t = t_{2\pi} = 2\pi/\omega$, the time required for the air-relative velocity vector to describe a full circle at the maximum turn rate.

Remark 1. There is a slight abuse of notation here in using the same path parameter t for both curves.

Let δ_i denote the sense of the turn for $i \in \{1, 2\}$. We seek the four feasible paths of shortest length corresponding to each of the four possible turn sequences ($\delta_1 \in \{-1, 1\}$ and $\delta_2 \in \{-1, 1\}$):

$$x_{t_1}(t) = \frac{V_a}{\delta_1 \omega} \sin(\delta_1 \omega t + \phi_{t_1}) + V_w t + x_{t_{10}} \tag{16}$$

$$y_{t_1}(t) = \frac{-V_a}{\delta_1 \omega} \cos(\delta_1 \omega t + \phi_{t_1}) + y_{t_{10}} \tag{17}$$

$$x_{t_2}(t) = \frac{V_a}{\delta_2 \omega} \sin(\delta_2 \omega t + \phi_{t_2}) + V_w t + x_{t_{20}} \tag{18}$$

$$y_{t_2}(t) = \frac{-V_a}{\delta_2 \omega} \cos(\delta_2 \omega t + \phi_{t_2}) + y_{t_{20}} \tag{19}$$

Let us denote the point at which the extremal path leaves the first trochoidal segment as point P_A and the point at which it reaches the second trochoidal segment as point P_B (see Fig. 5). Define t_A and t_B, relative to the two trochoidal segments, such that

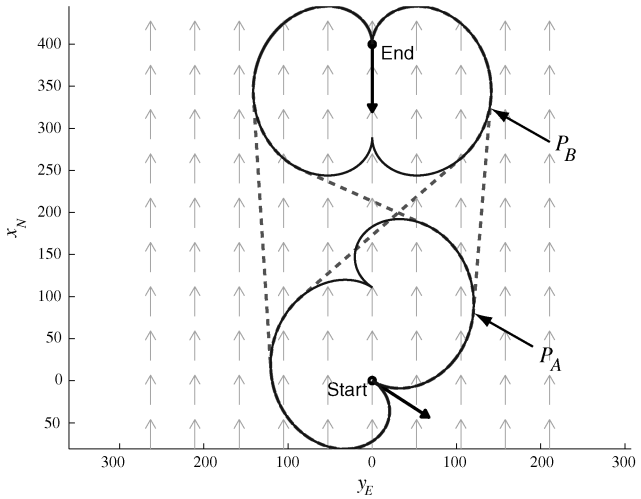

Fig. 5 Candidate extremal paths from the initial state to the final state (dashed lines) and trochoidal segments at the initial and final states plotted for $t \in [0, t_{2\pi}]$ (solid lines).

$$\begin{pmatrix} x_A \\ y_A \end{pmatrix} = \begin{pmatrix} x_{t_1}(t_A) \\ y_{t_1}(t_A) \end{pmatrix}, \qquad \begin{pmatrix} x_B \\ y_B \end{pmatrix} = \begin{pmatrix} x_{t_2}(t_B) \\ y_{t_2}(t_B) \end{pmatrix}$$

We pick the phase angles ϕ_{t_1} and ϕ_{t_2} such that the first trochoid has the desired initial heading ψ_0 at $t = 0$ and the second trochoid has the desired final heading ψ_f at $t = t_{2\pi}$:

$$\phi_{t_1} = \psi_0 - \psi_w, \qquad \phi_{t_2} = \psi_f - \psi_w - \delta_2 \omega t_{2\pi}$$

Similarly, we can pick the constants

$$x_{t_{10}} = x_0 - V_a/(\delta_1 \omega) \sin(\phi_{t_1}) \tag{20}$$

$$y_{t_{10}} = y_0 + V_a/(\delta_1 \omega) \cos(\phi_{t_1}) \tag{21}$$

$$x_{t_{20}} = x_f - V_a/(\delta_2 \omega) \sin(\delta_2 \omega t_{2\pi} + \phi_{t_2}) - V_w t_{2\pi} \tag{22}$$

$$y_{t_{20}} = y_f + V_a/(\delta_2 \omega) \cos(\delta_2 \omega t_{2\pi} + \phi_{t_2}) \tag{23}$$

such that the first trochoid satisfies the initial conditions

$$[x_{t_1}, y_{t_1}]^T|_{t=0} = [x_0, y_0]^T$$

and the second trochoid satisfies the final condition

$$[x_{t_2}, y_{t_2}]^T|_{t=t_{2\pi}} = [x_f, y_f]^T$$

Remark 2. Here, we assume that the initial and final conditions given in Eqs. (2) and (3) have been reexpressed in the trochoidal frame and denoted as $[x_0, y_0]^T$ and $[x_f, y_f]^T$.

With the preceding parameter definitions, and referring to Lemma 2, we seek the path parameters $t_A, \in [0, 2t_{2\pi})$, and $t_B \in (-t_{2\pi}, t_{2\pi}]$. The necessary conditions can be summarized as follows:

1) The velocities at point P_A and point P_B must be equal:

$$(\dot{x}_{t_1}(t_A), \dot{y}_{t_1}(t_A))^T = (\dot{x}_{t_2}(t_B), \dot{y}_{t_2}(t_B))^T \tag{24}$$

2) The line segment joining the points P_A and P_B must be tangent with the velocity vectors at both points:

$$\tan(\alpha) = \frac{y_{t_2}(t_B) - y_{t_1}(t_A)}{x_{t_2}(t_B) - x_{t_1}(t_A)} \tag{25}$$

$$\tan(\alpha) = \frac{\dot{y}_{t_2}(t_B)}{\dot{x}_{t_2}(t_B)} = \frac{\dot{y}_{t_1}(t_A)}{\dot{x}_{t_1}(t_A)} \tag{26}$$

3) The path parameters must satisfy

$$t_A \in [0, 2t_{2\pi}), \qquad t_B \in (-t_{2\pi}, t_{2\pi}] \tag{27}$$

Remark 3. For the case in which there is no wind ($V_w = 0$), one only needs to consider t_A and $t_B \in [0, t_{2\pi}]$, because $t_{2\pi}$ is the time it takes for the UAV to arrive back to its starting point. As shown in Sec. IV.C, this is not the case if winds are present.

Condition (24) is equivalent to the condition

$$\delta_1 \omega t_A + \phi_{t_1} = \delta_2 \omega t_B + \phi_{t_2} + 2k\pi, \qquad k \in \mathbb{Z}$$

where $\mathbb{Z}$ is the set of real integers, and we can express t_B as a function of t_A:

$$t_B = \frac{\delta_1}{\delta_2} t_A + \frac{\phi_{t_1} - \phi_{t_2} + 2k\pi}{\delta_2 \omega}, \qquad k \in \mathbb{Z} \tag{28}$$

Substituting Eq. (28) into Eq. (25), we get

$$\tan(\alpha) = \frac{(y_{t_{20}} - y_{t_{10}}) + \frac{\delta_2 - \delta_1}{\delta_1 \delta_2 \omega} V_a \cos(\delta_1 \omega t_A + \phi_{t_1})}{\frac{\delta_1 - \delta_2}{\delta_1 \delta_2 \omega} V_a \sin(\delta_1 \omega t_A + \phi_{t_1}) + (x_{t_{20}} - x_{t_{10}}) + V_w((\frac{\delta_1}{\delta_2} - 1)t_A + \frac{\phi_{t_1} - \phi_{t_2} + 2k\pi}{\delta_2 \omega})} \tag{29}$$

Because of condition (26), the tangent slope can also be expressed as

$$\tan(\alpha) = \frac{V_a \sin(\delta_1 \omega t_A + \phi_{t_1})}{V_a \cos(\delta_1 \omega t_A + \phi_{t_1}) + V_w}$$

Rearranging and using the identity $\sin^2\alpha + \cos^2\alpha = 1$, one gets the following implicit equation for t_A:

$$E \cos(\delta_1 \omega t_A + \phi_{t_1}) + F \sin(\delta_1 \omega t_A + \phi_{t_1}) = G \tag{30}$$

where

$$E = V_a \left(V_w \frac{\delta_1 - \delta_2}{\delta_1 \delta_2 \omega} - (y_{t_{20}} - y_{t_{10}}) \right) \tag{31}$$

$$F = V_a \left((x_{t_{20}} - x_{t_{10}}) + V_w \left(t_A \left(\frac{\delta_1}{\delta_2} - 1 \right) + \frac{\phi_{t_1} - \phi_{t_2} + 2k\pi}{\delta_2 \omega} \right) \right) \tag{32}$$

$$G = V_w (y_{t_{20}} - y_{t_{10}}) + \frac{V_a^2 (\delta_2 - \delta_1)}{\delta_1 \delta_2 \omega} \tag{33}$$

Equation (30) has one unknown: t_A. Having found t_A, one may solve for t_B using Eq. (28). Because Eq. (30) is transcendental, t_A must be found numerically, in general. However, the problem is significantly simplified if one assumes that

$$\text{sign}(\delta_1) = \text{sign}(\delta_2)$$

that is, that the two trochoids have the same sense.

A. Analytical Solution for LSL and RSR Trajectories

In the case that $\text{sign}(\delta_1) = \text{sign}(\delta_2)$, the expression for t_B in Eq. (28) becomes

$$t_B = t_A + \frac{\phi_{t_1} - \phi_{t_2} + 2k\pi}{\delta_2 \omega}, \qquad k \in \mathbb{Z} \tag{34}$$

Then Eq. (29) can be written as

$$\tan(\alpha) = \frac{-\frac{V_a}{\delta_2 \omega} \sin(\delta_2 \omega t_B + \phi_{t_2}) + y_{t_{20}} - (-\frac{V_a}{\delta_1 \omega} \sin(\delta_1 \omega t_A + \phi_{t_1}) + y_{t_{10}})}{\frac{V_a}{\delta_2 \omega} \sin(\delta_2 \omega t_B + \phi_{t_2}) + y_{t_{20}} + V_w t_B - (\frac{V_a}{\delta_1 \omega} \sin(\delta_1 \omega t_A + \phi_{t_1}) + y_{t_{10}} + V_w t_A)} = \frac{y_{t_{20}} - y_{t_{10}}}{x_{t_{20}} - x_{t_{10}} + V_w \frac{\phi_{t_1} - \phi_{t_2} + 2k\pi}{\delta_2 \omega}}$$

where $k \in \mathbb{Z}$. Using Eq. (24), one obtains the following simplified form of Eq. (30):

$$V_a \tan(\alpha) \cos(\delta_1 \omega t_A + \phi_{t_1}) - V_a \sin(\delta_1 \omega t_A + \phi_{t_1}) = -V_w \tan(\alpha) \tag{35}$$

To solve Eq. (35) for t_A, note that it can also be written in the form

$$-\frac{V_a}{\cos\alpha} \sin(\beta - \alpha) = -V_w \tan(\alpha)$$

where $\beta = \delta_1 \omega t_A + \phi_{t_1}$ and we have used the identity

$$\sin(\beta - \alpha) = \sin\beta \cos\alpha - \cos\beta \sin\alpha$$

Solving the preceding equation for β gives

$$\beta = \sin^{-1}\left(\frac{V_w}{V_a} \sin(\alpha) \right) + \alpha$$

Substituting back into the previous definition for β, with $\omega = 2\pi / t_{2\pi}$, gives

$$t_A = \frac{t_{2\pi}}{\delta_1 2\pi} \left[\sin^{-1}\left(\frac{V_w}{V_a} \sin(\alpha) \right) + \alpha - \phi_{t_1} + 2m\pi \right], \qquad m \in \mathbb{Z} \tag{36}$$

Using Eq. (34) one may also find t_B:

$$t_B = t_A + \frac{\phi_{t_1} - \phi_{t_2} + 2k\pi}{\delta_2 \omega}, \qquad k \in \mathbb{Z} \tag{37}$$

Example 1. To better understand the preceding result, consider a simple case in which there is no wind ($V_w = 0$). Consider the following initial and final conditions:

$$x_{N_0} = 0, \qquad y_{E_0} = 0, \qquad \psi_0 = 0, \qquad x_{N_f} = 0, \qquad y_{E_f} = 200$$
$$\psi_f = \pi$$

Take $k = m = 0$ so that $t_A = t_{2\pi}([0 + \alpha + 0]/2\pi)$. (The meaning of the integers k and m will be discussed presently.) The parameter α is the slope of the tangent line connecting the two trochoids and is measured from the same axis as the heading angle. In this example, the value of α is $\pi/2$ for both the LSL and RSR extremals, as shown in Fig. 6. One interpretation of Eq. (36) is that t_A is obtained by scaling $t_{2\pi}$ with $\alpha/2\pi \in [0, 1]$. In Fig. 6, the RSR solution is then a quarter turn to the right, $t_A = \frac{1}{4} t_{2\pi}$, followed by a straight segment, followed by another quarter turn to the right. (Note that $t_B = \frac{3}{4} t_{2\pi}$; recall that we measure the path parameter for the second trochoidal segment backward from this segment's end time at $t_{2\pi}$.)

Solutions for different values $m \in \mathbb{Z}$ correspond to parallel shifts of the path corresponding to $m = 0$ (see Fig. 7a). By Eq. (36), however, it is easy to see that there are only two values of m for which $t_A \in [0, 2t_{2\pi})$. It is convenient to take t_A from Eq. (36) modulo $t_{2\pi}$ to

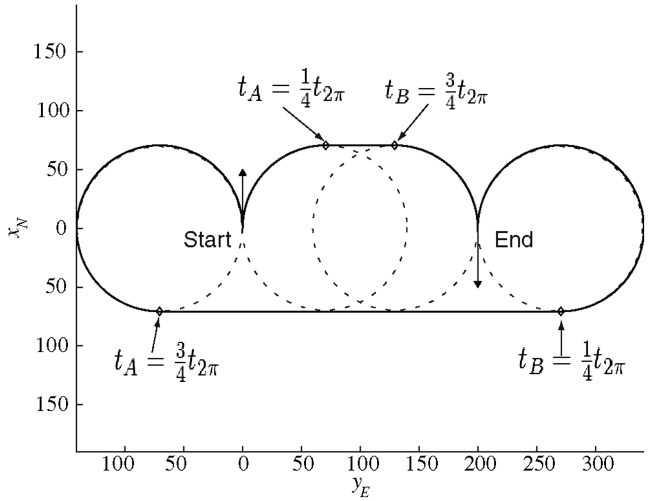

Fig. 6 Candidate extremals for $V_w = 0$. The figure illustrates how t_A is obtained by scaling $t_{2\pi}$ with $\alpha/2\pi \in [0, 1]$. In this case, $\alpha = \pi/2$. When turning left, $\delta_1 = -1$, so $t_A = -\frac{1}{4}t_{2\pi} \equiv \frac{3}{4}t_{2\pi}$.

obtain one of the solutions, call it t_{A_1}; the other solution is then $t_{A_2} = t_{A_1} + t_{2\pi}$. Consequently, we only consider $m = 0$.

The value of k affects the tangent angle α:

$$\alpha = \tan^{-1}\left(\frac{y_{t_{20}} - y_{t_{10}}}{x_{t_{20}} - x_{t_{10}} + V_w \frac{\phi_{t_1} - \phi_{t_2} + 2k\pi}{\delta_2 \omega}}\right), \qquad k \in \mathbb{Z}$$

This results in different solutions that connect the initial trochoid with a different loop of the final trochoid (see Fig. 7b). Assuming that $\phi_{t_1} - \phi_{t_2}$ is taken modulo 2π, it follows immediately from Eq. (34) that k can only take values in a finite set to ensure that $t_B \in (-t_{2\pi}, t_{2\pi}]$. For example, if $t_{A_1} \in [0, t_{2\pi})$ and $\delta_2 = 1$, this set is $k \in \{-2, -1, 0, 1\}$.

To obtain the most conservative bound on k, first consider $\delta_2 = 1$. In an imaginary worst case, when $t_A = 2t_{2\pi}$ and $\phi_{t_1} - \phi_{t_2} = 2\pi$, any $k < -3$ results in $t_B \leq -t_{2\pi}$, and so one only needs to consider $k \geq -3$. On the other hand, when $t_A = 0$ and $\phi_{t_1} - \phi_{t_2} = 0$, any $k > 1$ yields $t_B > t_{2\pi}$; hence, k has to take values in the set $k \in \{-3, -2, -1, 0, 1\}$. Similarly, when $\delta_2 = -1$, then k has to take values in $k \in \{-2, -1, 0, 1, 2\}$. The number of solutions that one needs to consider depends on t_A, δ_2, and $\phi_{t_1} - \phi_{t_2}$. In practice, it would be unnecessary to check the solutions for every value $k \in \{-3, \ldots, 2\}$. For the sake of generality, however, and because the solutions are trivial to compute, we consider all six possibilities in the following proposition.

Proposition 1. Define the path $\gamma(t)$ ($t \in [0, T]$), such that

$$\gamma(t) = \begin{pmatrix} x_{t_1}(t) \\ y_{t_1}(t) \end{pmatrix}, \qquad t \in [0, t_A]$$

$$\gamma(t) = \begin{pmatrix} x_{t_1}(t_A + \dot{x}_{t_1}(t_A)(t - t_A) \\ y_{t_1}(t_A) + \dot{y}_{t_1}(t_A)(t - t_A) \end{pmatrix}, \qquad t \in [t_A, t_\beta]$$

$$\gamma(t) = \begin{pmatrix} x_{t_2}(t - t_\beta + t_B) \\ y_{t_2}(t - t_\beta + t_B) \end{pmatrix}, \qquad t \in [t_\beta, T]$$

where

$$t_\beta = t_A + \frac{\sqrt{(x_{t_2}(t_B) - x_{t_1}(t_A))^2 + (y_{t_2}(t_B) - y_{t_1}(t_A))^2}}{\sqrt{\dot{x}_{t_2}(t_B)^2 + \dot{y}_{t_2}(t_B)^2}}$$

$$T = t_\beta + (t_{2\pi} - t_B)$$

and

$$\alpha = \tan^{-1}\left(\frac{y_{t_{20}} - y_{t_{10}}}{x_{t_{20}} - x_{t_{10}} + V_w \frac{\phi_{t_1} - \phi_{t_2} + 2k\pi}{\delta_2 \omega}}\right)$$

$$t_A = \frac{t_{2\pi}}{\delta_1 2\pi}\left[\sin^{-1}\left(\frac{V_w}{V_a}\sin(\alpha)\right) + \alpha - \phi_{t_1}\right]$$

$$t_B = t_A + \frac{\phi_{t_1} - \phi_{t_2} + 2k\pi}{\delta_2 \omega}, \qquad k \in \{-3, -2, -1, 0, 1, 2\}$$

The path $\gamma(t)$ satisfies the necessary conditions for time optimality. □

Remark 4. The final path that is selected by the algorithm satisfies the necessary conditions for optimality; however, one may not conclude optimality, in general, as there are additional extremal paths to consider: those for which the two trochoidal segments have the opposite sense (LSR and RSL) and, possibly, the BBB solutions. In the following, numerical root-finding methods are presented to find these other extremals.

B. Numerical Solution for LSR and RSL Trajectories

In the previous section, an analytical method was presented to find a subset of all possible candidate extremals (two out of six). Returning to Eq. (30), define the function

$$f(t_A) = E\cos(\delta_1 \omega t_A + \phi_{t_1}) + F\sin(\delta_1 \omega t_A + \phi_{t_1}) - G \qquad (38)$$

The objective is to find the values of t_A for which $f(t_A) = 0$. The function $f(t_A)/V_a V_w$ is plotted in Fig. 8 for the following boundary conditions and parameters:

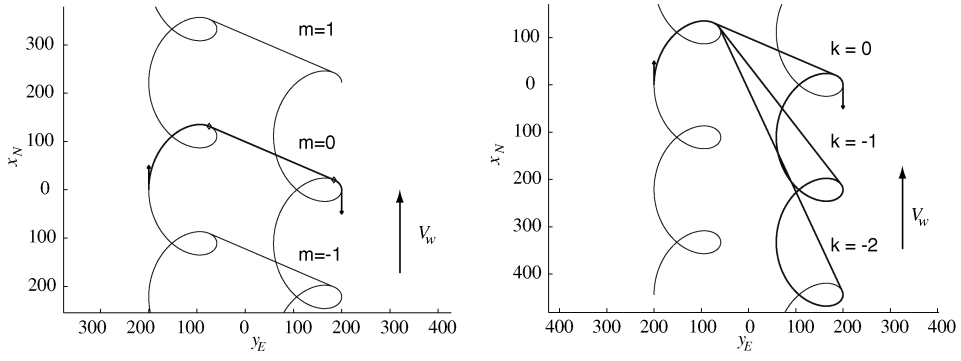

a) The effect of $m \in \mathbb{Z}$ **b) The effect of $k \in \mathbb{Z}$**

Fig. 7 The effect of $m \in \mathbb{Z}$ is a parallel shift with respect to the feasible solution. The effect of $k \in \mathbb{Z}$ is a variety of different tangent lines connecting the initial and final trochoids.

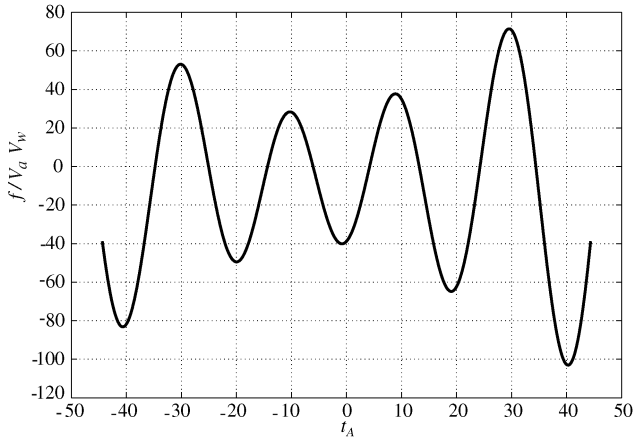

Fig. 8 The function $f(t_A)/V_a V_w$ for $t_A \in [-2t_{2\pi}, 2t_{2\pi}]$. There are several roots for $t_A \in [0, t_{2\pi}]$.

$$x_{N_0} = 0 \text{ m}, \qquad y_{E_0} = -200 \text{ m}, \qquad \psi_0 = 0, \qquad x_{N_f} = 0 \text{ m}$$
$$y_{E_f} = 200 \text{ m}, \qquad \psi_f = \pi \qquad V_a = 20 \text{ m/s}, \qquad V_w = 5 \text{ m/s}$$
$$\psi_w = 0$$

To find the roots of the equation $f(t_A) = 0$, one may use any root-finding technique, such as the bisection algorithm or the Newton–Raphson method; here, we consider the latter. Define the mapping

$$g(t_A) = t_A - \frac{f(t_A)}{f'(t_A)}$$

where

$$f'(t_A) = \frac{\mathrm{d}f(t_A)}{\mathrm{d}t_A} = -E\delta_1\omega\sin(\delta_1\omega t_A + \phi_{t_1}) + F\delta_1\omega\cos(\delta_1\omega t_A + \phi_{t_1}) + V_a V_w\left(\frac{\delta_1}{\delta_2} - 1\right)\sin(\delta_1\omega t_A + \phi_{t_1}) \tag{39}$$

If the initial guess $\hat{t}_{A_1}$ is close enough to the true solution t_A, then the map defined by

$$\hat{t}_{A_{i+1}} = g(\hat{t}_{A_i}), \qquad i = 1, 2, \ldots$$

is a contraction map. Then by the Banach fixed-point theorem, the series converges to t_A [10]. As illustrated in Fig. 8 as an example, there are several possible roots that one needs to consider. Some of these solutions are infeasible: those for which the straight segment would join and leave the trochoidal paths in the opposite sense. Although the Newton–Raphson method converges to the root only if the initial condition is close enough to the true solution, simulations suggest that the algorithm converges within three to six iterations, on average. Both functions in Eqs. (38) and (39) are simple smooth functions and are easy to compute; it is a simple matter to define a sufficiently dense grid of initial conditions on the interval $t_A \in [0, 2t_{2\pi}]$. Once a value for t_A is obtained, the corresponding value of t_B may be found using Eq. (28). If the obtained solution satisfies all the conditions (24–27), then the corresponding path is a candidate minimum-time trajectory. Results of Monte Carlo simulations are presented in Sec. VI.

As in the previous section, the number of possible solutions can be limited to a finite set to ensure that $t_B \in (-t_{2\pi}, t_{2\pi}]$. Because $\delta_1/\delta_2 = -1$, we have that $(\delta_1/\delta_2)t_A \in (-2t_{2\pi}, 0]$. Assuming that $\phi_{t_1} - \phi_{t_2}$ is taken modulo 2π, it follows from Eq. (28) that $k \in \{-1, 0, 1, 2, 3\}$. The distinct solutions may be entered into a table, along with the LSL and RSR paths obtained using the analytical expression discussed in Sec. IV.A. In cases in which BBB solutions do not exist, the true minimum-time solution is picked from these candidates. Although the approach described previously employs a numerical root-finding algorithm, the simple closed-form expressions and the small number of required iterations make the runtime predictable and quick (see Sec. VI). The algorithm is quite suitable for implementation as a real-time UAV path-planning method.

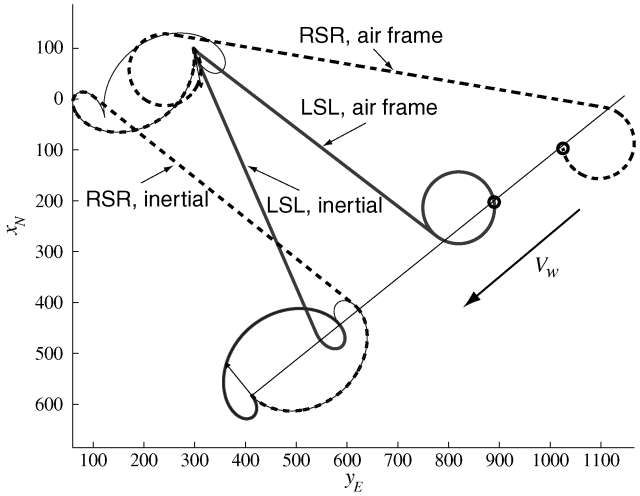

Fig. 9 Illustration showing that for some initial conditions, some of the extremals fail to satisfy $t_B \in [0, t_{2\pi}]$. In this example, $t_B < 0$ for the LSL trajectory. The figure shows both the inertial path and the air-relative path. The circles indicate the position of a virtual target [5], traveling upwind with the same speed as the wind speed, that the aircraft would intercept by flying a minimum-time path in the air-relative frame.

This simple numerical routine yields those candidate extremals for which the trochoids have opposite sense [i.e., $\text{sign}(\delta_1) \neq \text{sign}(\delta_2)$]. Examples of candidate minimum-time BSB trajectories for randomly selected initial and final conditions are discussed in Sec. VI.

C. Existence of Unconventional Extremals

Consider the case in which there is no wind or, equivalently, the problem of finding the shortest paths of bounded curvature in the plane [1–3]. In the absence of wind, the trochoidal segments become circular. In this case, a UAV turning at maximum rate would arrive back to its original position in exactly time $t_{2\pi}$, and so it is unnecessary to consider solutions for which $t_A, t_B \notin [0, t_{2\pi}]$. Moreover, the following lemma is proved in [3].

Lemma 3 [3]. Denote the angle of intermediate arcs on the circular segments by u and v. A path $R_u S R_v$, or $L_u S L_v$, cannot be optimal if $u + v > 2\pi$.

The equivalent of this lemma in the case in which winds are present would state that for an optimal path, $t_A + (t_{2\pi} - t_B) \leq t_{2\pi}$. In other words, the total time spent on both trochoidal segments must be no greater than $t_{2\pi}$ for optimality.

Every extremal in the inertial frame has a corresponding airframe equivalent, which is the UAV path that an observer moving with the wind would see. In the air-relative frame, the extremals are composed of circular segments and straight lines. For the purpose of this section, we call extremals conventional if there exists a corresponding minimum-time Dubins path in the air-relative frame $\mathcal{F}_A$. By Dubins path we mean any minimum arc-length path as described in [1]. It turns out, however, that if $V_w \neq 0$, then extremals in the inertial frame may not be Dubins paths in the air-relative frame. This is illustrated by the following example.

Consider the initial and final conditions and parameters

$$x_{N_0} = 101.3 \text{ m}, \qquad y_{E_0} = 297.1 \text{ m}, \qquad \psi_0 = 2.48$$
$$x_{N_f} = -581.47 \text{ m}, \qquad y_{E_f} = 411.29 \text{ m}, \qquad \psi_f = 6.12$$
$$V_a = 20 \text{ m/s}, \qquad V_w = 10 \text{ m/s}, \qquad \psi_w = 4.04$$
$$\omega = 0.2832$$

In Fig. 9, we can see the resulting LSL and RSR trajectories. For the LSL path (solid line), there is no solution that would satisfy both

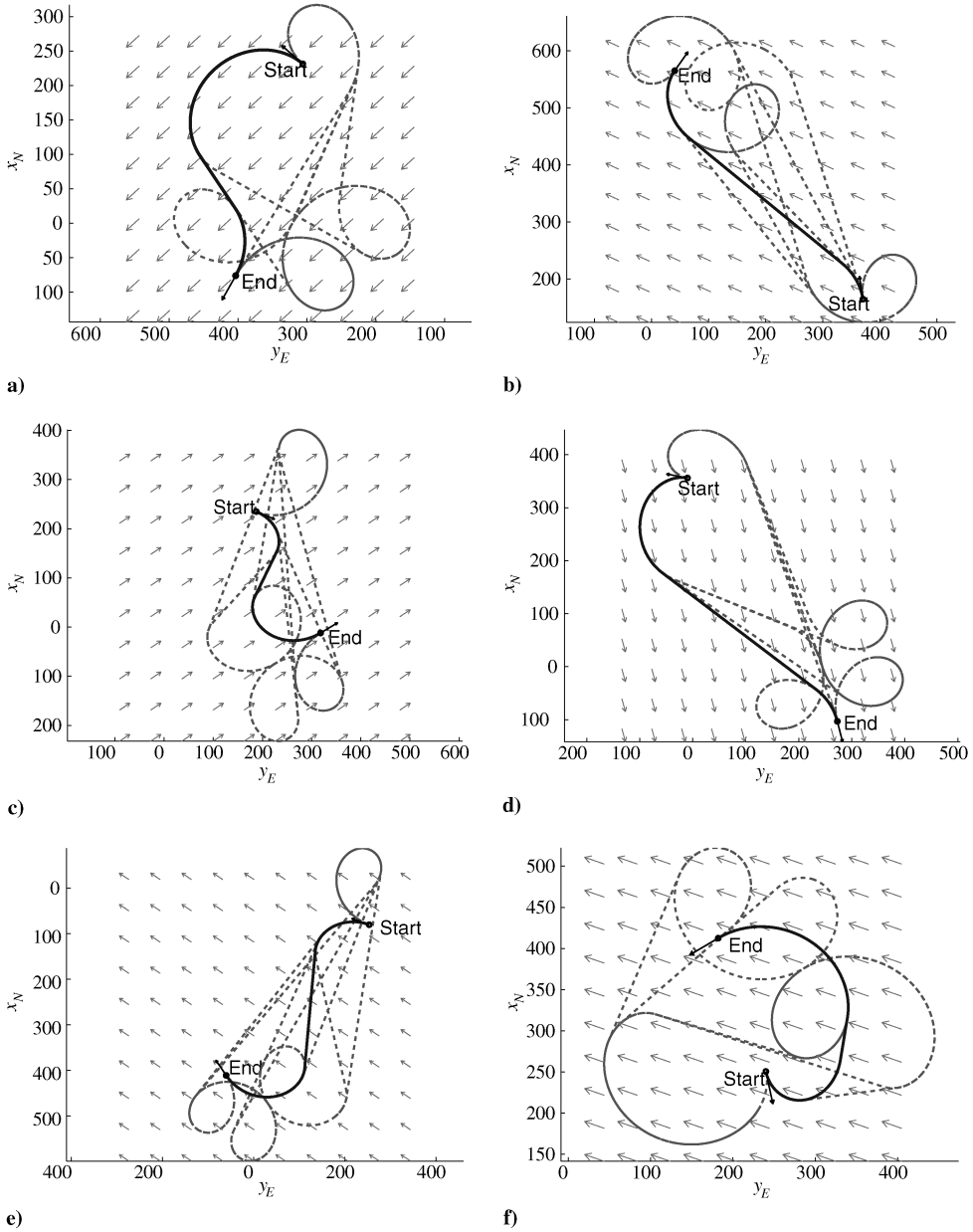

Fig. 10 Candidate BSB extremal paths for randomly selected initial and final states.

$t_A \in [0, t_{2\pi}]$ and $t_B \in [0, t_{2\pi}]$. This is due to the fact that the instantaneous center of the maximum turn rate circle in the air-relative frame moves distance $d = V_w t_{2\pi}$ in the direction of the wind in time $t_{2\pi}$. Thus, we have established the following.

Proposition 2. There exist initial and final conditions (x_0, y_0, ψ_0) and (x_f, y_f, ψ_f) and parameter values V_a, V_w, ψ_w, and ω for which some of the candidate extremals fail to satisfy that both $t_A \in [0, t_{2\pi}]$ and $t_B \in [0, t_{2\pi}]$. □

An immediate consequence of Proposition 2 is that if one were to look for minimum-time paths in the inertial frame by looking for their corresponding minimum-time equivalent in the air-relative frame, some of the possible extremals would not be found. Referring to Fig. 9, the RSR path would be easily found, but the LSL path would be missed, as its airframe equivalent is not a Dubins trajectory.

V. Solving for BBB Trajectories

As in the previous section, we define three trochoids as

$$x_{t_1}(t) = \frac{V_a}{\delta_1 \omega} \sin(\delta_1 \omega t + \phi_{t_1}) + V_w t + x_{t_{10}}, \qquad t \in [0, t_A] \quad (40)$$

$$y_{t_1}(t) = \frac{-V_a}{\delta_1 \omega} \cos(\delta_1 \omega t + \phi_{t_1}) + y_{t_{10}} \quad (41)$$

$$x_{t_2}(t) = \frac{V_a}{\delta_2 \omega} \sin(\delta_2 \omega t + \phi_{t_2}) + V_w t + x_{t_{20}}, \qquad t \in [t_A, t_B] \quad (42)$$

$$y_{t_2}(t) = \frac{-V_a}{\delta_2 \omega} \cos(\delta_2 \omega t + \phi_{t_2}) + y_{t_{20}} \quad (43)$$

$$x_{t_3}(t) = \frac{V_a}{\delta_3 \omega} \sin(\delta_3 \omega t + \phi_{t_3}) + V_w t + x_{t_{30}}, \qquad t \in [t_B, T] \quad (44)$$

$$y_{t_3}(t) = \frac{-V_a}{\delta_3 \omega} \cos(\delta_3 \omega t + \phi_{t_3}) + y_{t_{30}} \quad (45)$$

where $\delta_i \in \{-1, 1\}$, with $\delta_1 = \delta_3 = -\delta_2$.

Remark 5. Note that here the path parameter value is common for all three segments (cf. Remark 1).

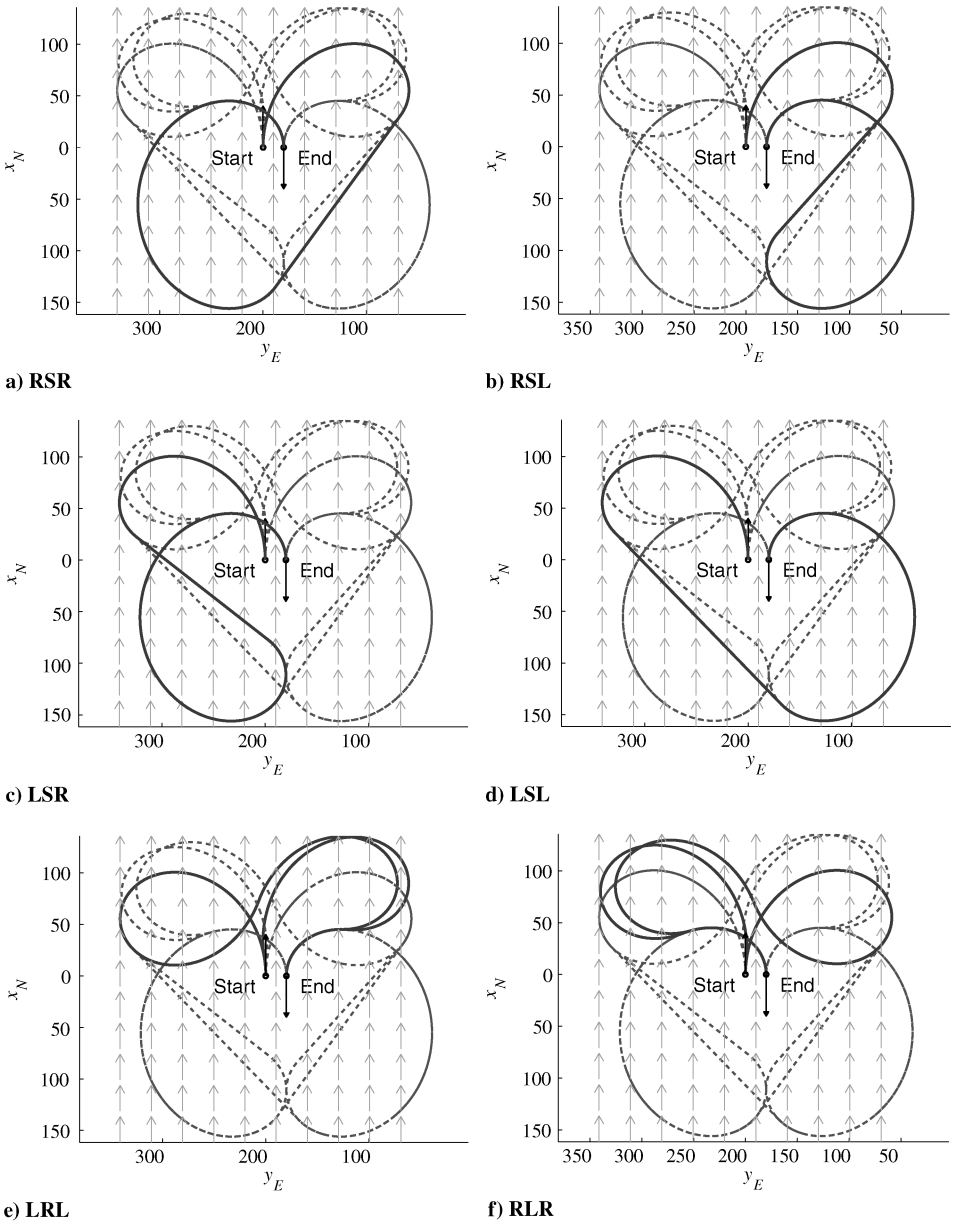

Fig. 11 Candidate time-optimal paths found by the path-planning algorithm for initial conditions $x_0 = 0$ m, $y_0 = -200$ m, $\psi_0 = 0$, $x_f = 0$ m, $y_f = -180$ m $\psi_f = \pi$, $\omega = 0.2832$ rad/s, $V_w = 5$ m/s, and $V_a = 20$ m/s. The time-optimal path is LRL trajectory with $t_A = 0.6869$ s, $t_B = 17.4451$ s, and $T = 22.4228$ s. Note that for the LRL and RLR paths there are two extremals to consider: they both satisfy the necessary conditions for optimality.

The objective is to find the path parameter values t_A, t_B, and T and the integration constants $x_{t_{i0}}$, $y_{t_{i0}}$, and ϕ_{t_i}, such that

$$[x_{t_1}, y_{t_1}, \psi_{t_1}]^T|_{t=0} = [x_0, y_0, \psi_0]^T$$

and

$$[x_{t_3}, y_{t_3}, \psi_{t_3}]^T|_{t=T} = [x_f, y_f, \psi_f]^T$$

where $\psi_{t_i} = \delta_i \omega t + \phi_{t_i}$.

The problem can be simplified to obtain two transcendental equations for two unknowns t_A and T. The system of equations can be solved using a numerical root-finding technique to obtain t_A and T. Examples of candidate minimum-time BSB trajectories are discussed in Sec. VI. The details of the calculation are presented in the Appendix.

VI. Results

The methods described in the preceding sections were tested in Monte Carlo simulations. The aircraft airspeed was $V_a = 20$ m/s, the wind speed was $V_w = 5$ m/s, and the maximum turn rate was $\omega = 0.2832$ rad/s, which corresponds to a maximum bank angle $\phi_{\max} = 30$ deg for an aircraft in a coordinated turn. The boundary conditions were randomly selected from uniform distributions over the ranges shown in Table 1.

The path-planning algorithm was executed for $N = 10,000$ randomly selected initial and final points. The average runtime on a 2.66 GHz CPU was $T_{\text{avg}_{\text{run}}} = 308$ ms with standard deviation $\sigma_{\text{run}} = 18$ ms. The distribution of path types is shown in Table 2. In the case when only the BSB trajectories are calculated, the runtime reduces to $T_{\text{avg}_{\text{run}}} = 3.2$ ms. The grid size for solving Eq. (38) was $N_i = 10$ for these simulations (Sec. IV.B). For the 2-D Newton–Raphson method, this results in $N_{i_{2D}} = 10 \times 10 = 100$ initial points for the root-finding algorithm, explaining the increased runtime. It is well known that the BBB Dubins paths in the absence of winds only exist if the distance between the initial and final points satisfies $d \leq 4R_0$, where R_0 is the maximum-rate turning radius. Thus, if it is known that the initial and final points are sufficiently far from each other, one only needs to consider the BSB paths.

Table 1 Initial conditions selected randomly

Condition	Range
x_{N_0}	−500 to 500 m
y_{E_0}	−500 to 500 m
ψ_0	0 to 2π
ψ_f	0 to 2π
ψ_w	0 to 2π
R[a]	−500 to 500 m
θ[a]	0 to 2π

[a]The final point was selected R distance away from the initial point in the direction defined by θ.

Table 2 Distribution of minimum-time path types based on Monte Carlo simulations

Path type	Distribution
LSL	26%
RSR	25%
LSR	19.6%
RSL	19.9%
RLR	4.9%
LRL	4.6%

Figure 10 shows the results for the BSB solutions only, for randomly selected initial and final conditions. In the figures, the initial conditions and parameters were selected the same way as in the Monte Carlo simulations. The dashed lines show the candidate extremals for the LSL, RSL, LSR, and RSR trajectories, and the solid line shows the minimum-time path selected among these candidate extremals.

Figure 11 shows the results for all possible three-segment extremals. In the example, the initial conditions were selected as $x_0 = 0$ m, $y_0 = -200$ m, $\psi_0 = 0$, $x_f = 0$ m, $y_f = -180$ m, and $\psi_f = \pi$, and the parameters used for the path-planning algorithm were $\omega = 0.2832$ rad/s, $V_w = 5$ m/s, and $V_a = 20$ m/s. Figs. 11a–11f show all candidate extremals as a dashed line. The difference between the figures is that each has only a set of extremals highlighted in a solid line, corresponding to the RSR, RSL, LSR, LSL, LRL, and RLR trajectories, respectively. In this case, the minimum-time trajectory is the one highlighted with a solid line in Fig. 12, which is a slight initial turn to the left, followed by a turn to the right, then followed by another turn to the left.

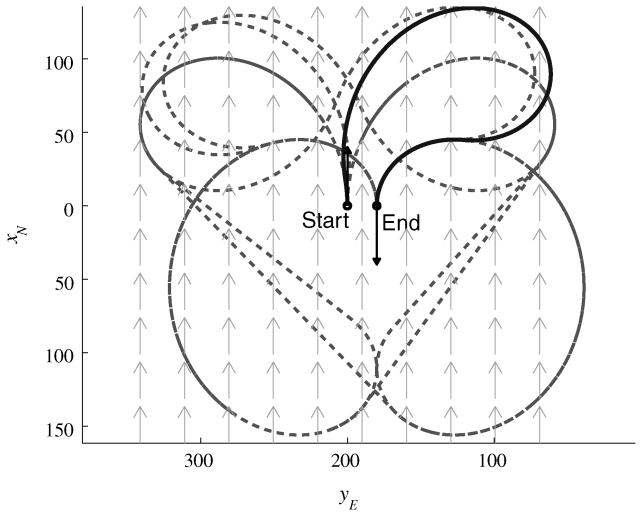

Fig. 12 Candidate time-optimal paths found by the path-planning algorithm for initial conditions $x_0 = 0$ m, $y_0 = -200$ m, $\psi_0 = 0$, $x_f = 0$ m, $y_f = -180$ m $\psi_f = \pi$, $\omega = 0.2832$ rad/s, $V_w = 5$ m/s, and $V_a = 20$ m/s. The time-optimal path is LRL trajectory with $t_A = 0.6869$ s, $t_B = 17.4451$ s, and $T = 22.4228$ s.

VII. Conclusions

In this paper, we presented a minimum-time path-planning procedure for constant-speed UAVs flying in the presence of steady uniform winds. We assume that environmental parameters such as wind speed and direction and the given initial conditions and prescribed final conditions are known. The contribution of the work is the development of a framework that allows to solve for a subset of all candidate solutions in closed form. The analytical solutions and efficient numerical root-finding routines suggest the method's suitability for real-time implementation on unmanned systems' onboard computers with limited computational capacities. The efficiency of the path-planning algorithm is supported with exhaustive Monte Carlo simulations.

Although the methods presented in this paper were developed for UAVs flying in constant winds, we anticipate that they will find broader use in other autonomous vehicle applications in which the vehicles travel with constant speed and the assumption of a steady uniform external flowfield is reasonable. Examples of such applications include autonomous underwater vehicles in ocean currents or autonomous surface vehicles in riverine operations.

Appendix: Solving for BBB Trajectories

Consider Eqs. (40–45), where $\delta_i \in \{-1, 1\}$, with $\delta_1 = \delta_3 = -\delta_2$. We seek the path parameter values t_A, t_B, and T and the integration constants $x_{t_{i0}}$, $y_{t_{i0}}$, and $\phi_{t_{i0}}$, such that

$$[x_{t_1}, y_{t_1}, \psi_{t_1}]^T|_{t=0} = [x_0, y_0, \psi_0]^T$$

and

$$[x_{t_3}, y_{t_3}, \psi_{t_3}]^T|_{t=T} = [x_f, y_f, \psi_f]^T$$

where $\psi_{t_i} = \delta_i \omega t + \phi_{t_i}$. From the initial conditions, we can determine $x_{t_{10}}$, $y_{t_{10}}$, and ϕ_{t_1} as

$$x_{t_{10}} = x_0 - V_a/(\delta_1 \omega)\sin(\phi_{t_1}) \tag{A1}$$

$$y_{t_{10}} = y_0 - V_a/(\delta_1 \omega)\cos(\phi_{t_1}) \tag{A2}$$

$$\phi_{t_1} = \psi_0 \tag{A3}$$

From the final condition, we have

$$x_{t_{30}} = x_f - V_a/(\delta_3 \omega)\sin(\psi_f) - V_w T \tag{A4}$$

$$y_{t_{30}} = y_f + V_a/(\delta_3 \omega)\cos(\psi_f) \tag{A5}$$

$$\phi_{t_3} = \psi_f - \delta_3 \omega T \tag{A6}$$

We are left with six unknowns: $x_{t_{20}}$, $y_{t_{20}}$, ϕ_{t_2}, t_A, t_B, and T. One may write a total of six continuity equations at points t_A and t_B (two for position and one for heading at each point) as follows:

$$x_{t_1}(t_A) = x_{t_2}(t_A), \qquad x_{t_2}(t_B) = x_{t_3}(t_B) \tag{A7}$$

$$y_{t_1}(t_A) = y_{t_2}(t_A), \qquad y_{t_2}(t_B) = y_{t_3}(t_B) \tag{A8}$$

$$\psi_{t_1}(t_A) = \psi_{t_2}(t_A), \qquad \psi_{t_2}(t_B) = \psi_{t_3}(t_B) \tag{A9}$$

From Eq. (A9) and noting that $\delta_1 = -\delta_2$, one may write

$$\phi_{t_2} = 2\delta_1 \omega t_A + \phi_{t_1}$$

$$t_B = \frac{\psi_f + \delta_2 \omega T - \phi_{t_2}}{2\delta_2 \omega} = t_A + \frac{T}{2} + \frac{\psi_f - \psi_0}{2\delta_2 \omega} \tag{A10}$$

From Eqs. (A7) and (A8), we can write four additional continuity equations:

$$\begin{pmatrix} x_{t_{20}} \\ y_{t_{20}} \end{pmatrix} = \begin{pmatrix} x_{t_{30}} - 2\frac{V_a}{\delta_2 \omega} \sin(\delta_2 \omega t_B + \phi_{t_2}) \\ y_{t_{30}} + 2\frac{V_a}{\delta_2 \omega} \cos(\delta_2 \omega t_B + \phi_{t_2}) \end{pmatrix} \tag{A11}$$

$$\begin{pmatrix} x_{t_{10}} \\ y_{t_{10}} \end{pmatrix} = \begin{pmatrix} x_{t_{20}} + 2\frac{V_a}{\delta_2 \omega} \sin(\delta_2 \omega t_A + \phi_{t_2}) \\ y_{t_{20}} - 2\frac{V_a}{\delta_2 \omega} \cos(\delta_2 \omega t_A + \phi_{t_2}) \end{pmatrix} \tag{A12}$$

Substituting $x_{t_{30}}$ and $y_{t_{30}}$ from Eqs. (A4) and (A5) into Eq. (A11) and then $x_{t_{20}}$ and $y_{t_{20}}$ from Eqs. (A11) and (A12) and using expressions (A10), we obtain two transcendental equations for t_A and T:

$$\mathbf{f}(t_A, T) = \begin{pmatrix} \frac{2V_a}{\delta_1 \omega} \sin(\delta_1 \omega t_A + \phi_{t_1}) + x_{t_{10}} - x_{t_{30}} + \frac{2V_a}{\delta_2 \omega} \sin(\delta_2 \omega \frac{T}{2} + \frac{\psi_f}{2} + \delta_1 \omega t_A + \frac{\phi_{t_1}}{2}) \\ -\frac{2V_a}{\delta_1 \omega} \cos(\delta_1 \omega t_A + \phi_{t_1}) + y_{t_{10}} - y_{t_{30}} - \frac{2V_a}{\delta_2 \omega} \cos(\delta_2 \omega \frac{T}{2} + \frac{\psi_f}{2} + \delta_1 \omega t_A + \frac{\phi_{t_1}}{2}) \end{pmatrix} \equiv \mathbf{0}$$

where $x_{t_{30}}(T)$ and $y_{t_{30}}(T)$ depend on T as in Eqs. (A4) and (A5). The roots of the equations can be found using a second-order Newton–Raphson method. Define the mapping

$$g(t_A, T) = \begin{pmatrix} t_A \\ T \end{pmatrix} - \mathbf{J}^{-1}(t_A, T)\mathbf{f}(t_A, T)$$

where

$$\mathbf{J}(t_A, T) = \begin{bmatrix} \frac{\partial f_1}{\partial t_A}(t_A, T) & \frac{\partial f_1}{\partial T}(t_A, T) \\ \frac{\partial f_2}{\partial t_A}(t_A, T) & \frac{\partial f_2}{\partial T}(t_A, T) \end{bmatrix}$$

is the Jacobian matrix. If the initial guess $(t_{A_0}, T_0)^T$ is close enough to the true solutions, then the mapping defined by

$$\begin{pmatrix} t_{A_{i+1}} \\ T_{i+1} \end{pmatrix} = \mathbf{g}(t_{A_i}, T_i)$$

converges to the root. In case the Jacobian matrix becomes singular, the root-finding algorithm may be started with a different initial condition.

Acknowledgments

This work was sponsored by the U.S. Office of Naval Research under grant nos. N00014-08-1-0012 and N00014-08-1-0778. The authors gratefully acknowledge the constructive comments of the anonymous reviewers.

References

[1] Dubins, L. E., "On Curves of Minimal Length with a Constraint on Average Curvature, and with Prescribed Initial and Terminal Positions and Tangents," *American Journal of Mathematics*, Vol. 79, No. 3, 1957, pp. 497–516. doi:10.2307/2372560

[2] Boissonat, J. D., Cerezo, A., and Leblond, J., "Shortest Paths of Bounded Curvature in the Plane," *Proceedings of the IEEE International Conference on Robotics and Automation*, Inst. of Electrical and Electronics Engineers, Piscataway, NJ, May 1992, pp. 2315–2320.

[3] Bui, X., Soukres, P., Boissonnat, J. D., and Laumond, J. P., "Shortest Path Synthesis for Dubins Non-Holonomic Robot," *IEEE International Conference on Robotics and Automation*, Inst. of Electrical and Electronics Engineers, Piscataway, NJ, 1994, pp. 2–7.

[4] McGee, T. G., Spry, S., and Hedrick, J. K., "Optimal Path Planning in a Constant Wind with a Bounded Turning Rate," AIAA Guidance Navigation, and Control Conference and Exhibit, San Francisco, AIAA, Paper 2005-6186, Aug. 2005.

[5] McGee, T. G., and Hedrick, J. K., "Optimal Path Planning with a Kinematic Airplane Model," *Journal of Guidance, Control, and Dynamics*, Vol. 30, No. 2, 2007, pp. 629–633. doi:10.2514/1.25042

[6] Rysdyk, R. T., "Course and Heading Changes in Significant Wind," *Journal of Guidance, Control, and Dynamics*, Vol. 30, No. 4, 2007, pp. 1168–1171. doi:10.2514/1.27359

[7] Techy, L., Woolsey, C. A., and Schmale, D. G., III, "Path Planning for Efficient UAV Coordination in Aerobiological Sampling Missions," *Proceedings of the 47th IEEE Conference on Decision and Control*, Inst. of Electrical and Electronics Engineers, Piscataway, NJ, Dec. 2008, pp. 2814–2819.

[8] Bestaoui, Y., Dahmani, H., and Belharet, K., "Geometry of Translational Trajectories for an Autonomous Aerospace Vehicle with Wind Effect," 47th AIAA Aerospace Sciences Meeting, Orlando, FL, AIAA, Paper 2009-1352, Jan. 2009.

[9] Sussmann, H. J., and Tang, G., "Shortest Paths for the Reeds-Shepp Car: A Worked Out Example of the Use of Geometric Techniques in Nonlinear Optimal Control," *Rutgers Center for Systems and Control*, Rept. SYCON 91-10, New Brunswick, NJ, 1991.

[10] Miller, P. D., *Applied Asymptotic Analysis*, 1st ed., American Mathematical Society, Providence, RI, 2006, pp. 232–234.